Original Article

Institution of MECHANICAL ENGINEERS
Journal of MECHANICAL ENGINEERING SCIENCE

Design of a master device for controlling multi-moduled continuum robots

Proc IMechE Part C:
J Mechanical Engineering Science
2017, Vol. 231(10) 1921–1931

DOI: 10.1177/0954406215625359
journals.sagepub.com/home/pic
SAGE

Hyun-Soo Yoon[1] and Byung-Ju Yi[2]

Abstract

Few interface systems designed to control continuum robots have been developed. This work presents a master device for multi-unit continuum robots. The master mechanism has the same kinematic structure as the slave device. The kinematic structure, which uses a spring as a backbone, allows for a unique forward kinematic solution. This design is slim-sized, light-weight, and easy to implement. As an example mechanism, a continuum unit with two degrees of freedom was developed. Two-unit modules were assembled to generate four degrees of freedom. The performance of the master device is verified through a master-slave control experiment.

Keywords

Master device, continuum, forward kinematics

Date received: 30 July 2015; accepted: 7 December 2015

Introduction

Continuum robots have been developed for various application areas. Ikuta et al.[1,2] developed a hyper redundant miniature manipulator for minimally invasive surgery. Each miniature manipulator has nine degrees of freedom (DOF) and is controlled by a wire. Simaan[3–5] presented a snake-like continuum unit using a flexible backbone and push-pull-type wire actuation. Camarillo et al.[6] presented a tendon-driven continuum manipulator. Walker et al.[7–11] developed an elephant's trunk manipulator. This continuum style robot has a large number of degrees of freedom and a wide range of maneuverability. Webster et al. and Dupont et al.[12–16] developed a continuum robot by using multiple pre-curved concentric tubes. These devices derive bending actuation from elastic energy stored in the backbone itself. Choi et al.[17] presented a design for a spring backbone micro-endoscope, and Yoon et al.[18,19] developed a continuum robot that employs a spring as its backbone for use in nose surgeries.

Although there are many studies that have investigated continuum robots, research related to interface system design to control continuum robots has been very limited. This is due to the complex kinematic structure of continuum robots. Thus, coming up with a simple interface design for operators is much less intuitive as compared to controlling serial-type robots. Therefore, a proper user interface that is both intuitive to operators and easy to use should be developed. One possible way to create a user interface that is both intuitive and easy to control would be to give the master and the slave robot the same kinematic structure.

Walker et al.[20] proposed a user interface for continuum robot arms, but they used a joystick as the master device to control the arms. If the user intends to control only the end point of the slave robot, a joystick interface is acceptable and useful. However, in the case of control of the entire shape of the continuum robot, a joystick interface is non-intuitive to operators and not an appropriate method for properly controlling the whole shape of the continuum robot because the structure of the master device is different from that of the slave robot.

In this paper, a master device that is assembled by multiple continuum units is proposed. Each continuum unit is similar to a parallel kinematic mechanism that has a unique forward kinematic solution. Thus, it is used as a master device to control a slave robot with the same kinematic structure. In Forward Kinematics of a 4-Degrees Of Freedom (DOF) Continuum Robot section, we present the forward kinematic solution of a 4-DOF continuum robot consisting of two continuum units. Design of this master

[1]Department of Electronic, Electrical, Control and Instrumentation Engineering, Hanyang University, Korea
[2]Department of Electronic Systems Engineering, Hanyang University, Korea

Corresponding author:
Byung-Ju Yi, Department of Electronic Systems Engineering, Hanyang University, Korea.
Email: bj@hanyang.ac.kr

device is presented in Design of a Master Device to Control a 4-DOF Continuum Robot section. In Implementation section, the performance of the master device is verified through a master-slave control experiment. Finally, we draw our conclusions in Conclusion section.

Forward kinematics of a 4-DOF continuum robot

Structure of a 4-DOF flexible continuum robot

The kinematic structure of the proposed 4-DOF flexible continuum robot was presented in previous work[21,22]; these describe the inverse kinematic modeling of the slave device. The proposed 4-DOF flexible continuum robot consists of two-unit modules. Each unit module has two DOF. Figure 1 shows the structure of this mechanism. Each unit module consists of a backbone spring and aluminum cylinders. To control each unit module, the cylinders are connected by wires through four holes pierced in the cylinders. Two rotational motions can be obtained by pulling and releasing the four wires.

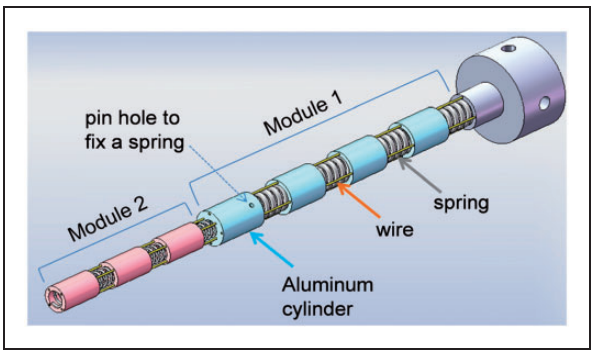

Figure 1. Structure of the 4-DOF flexible continuum robot.

Figure 2 shows the shape change of the mechanism and the deflection of a unit spring backbone that is caused by pulling the wires. As shown in Figure 2(a), a node consists of a unit spring backbone and one aluminum cylinder. It is assumed that the center line L_c maintains a constant value because of the symmetry of the unit spring backbone. Additionally, θ_v denotes the angle change of the backbone module; this is the same at every unit spring backbone.

The motion of each continuum unit module can be described by two rotation variables (β_1, γ). Initially, the continuum unit module is rotated with respect to the global $\hat{Y}$-axis by β_1. Next, the whole mechanism is rotated about the global $\hat{Z}$-axis by γ. Figure 3 shows the configuration of the spatial model as it is bent and rotated.

Here, we set β_1 and γ as the output variables of the continuum unit module. The lengths of the two wires are the input variables.

Figure 4 shows the bending plane; here, the relationship between the deflection angle θ_v of every spring module and the bending angle β_1 of the continuum unit is described as

$$\beta_1 = 2N\theta_v \tag{1}$$

where N is the number of nodes in one continuum unit.

Forward kinematics

Let us define ${}_1\beta_1$ and ${}_1\gamma$ as the output angles of the first continuum unit and ${}_2\beta_1$ and ${}_2\gamma$ as the output angles of the second continuum unit. Then, the forward kinematics can find these four output variables of the mechanism for the given sensor information of the input variables (${}_1l_1$, ${}_1l_2$, ${}_2l_1$, and ${}_2l_2$). Since each unit module of the continuum robot is designed

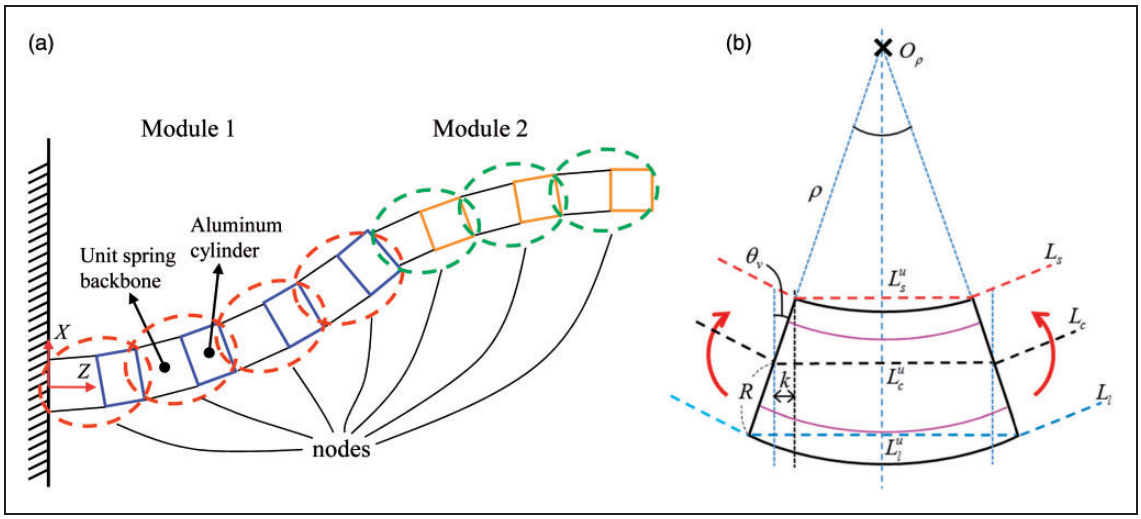

Figure 2. Side view of the 4-DOF flexible continuum robot. (a) Shape change of the 4-DOF flexible continuum robot. (b) Deflection of a unit spring backbone.

symmetrically, deflection will occur uniformly in every node of each unit module. Thus, analysis of one node could lead the kinematics for the whole continuum robot. Figure 5 shows the spatial model of the unit spring backbone.

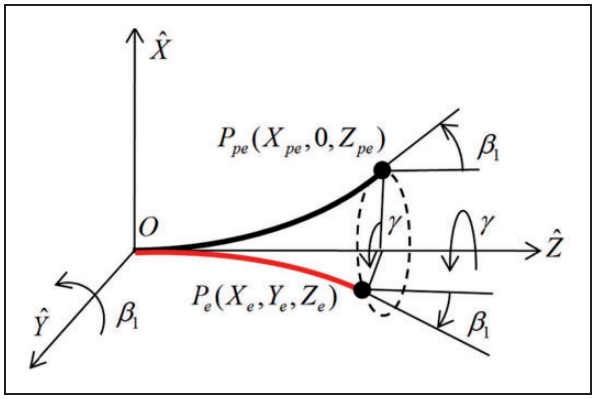

Figure 3. The bent and rotated shape of the spatial model.

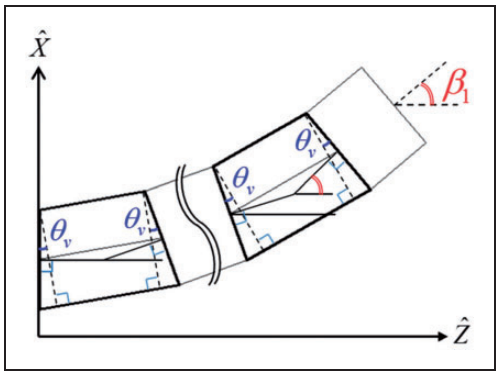

Figure 4. Relationship between β_1 and θ_v in the bending plane.

Figure 5(a) denotes the initial shape of the unit spring backbone without any rotation. The wire is modeled as a 5-DOF serial chain, and the center line of the unit spring backbone is modeled as a 4-DOF serial chain since the center length L_c^u of the unit spring backbone is constant. It is noted from Figure 5(b) that the four wires are arranged 90° apart at the base cylinder plate, and two wires (i.e. L_1^u and L_2^u) hit the x- and y-axis at p_1^b and p_2^b, respectively. Here, only two neighboring wires are necessary for position analysis, since the motion of the other two wires are dependent as described in literature.[21] When the unit spring backbone is bent, there are two isosceles trapezoids ($o^t p_1^t p_1^b o^b$ and $o^t p_2^t p_2^b o^b$) in the spatial model due to the symmetry of the unit spring backbone. In Figure 5(c), if the x- and y-positions of the center point (o^t) of the top plate are obtained, the bending angle θ_v of the unit spring backbone and the azimuth angle γ of the bending plane can be calculated.

In Figure 6, the two isosceles trapezoids are depicted in detail. One hypotenuse of the two trapezoids lies on x- and y-axis, respectively. L_1^u and L_2^u, which are the unit lengths of wires l_1 and l_2, are given as the input variables, and R is the cylinder radius of the continuum mechanism. From the geometry of Figure 6, the x- and y-positions of o^t can be obtained and expressed as

$$x = L_c^u \cos\psi_x \tag{2}$$

$$y = L_c^u \cos\psi_y \tag{3}$$

where

$$\psi_x = \begin{cases} \cos^{-1}\left(\overline{o^b p_1^{b'}}/R\right), & L_1^u < L_c^u \\ 180^\circ - \cos^{-1}\left(\overline{p_1^b o_x^{b'}}/R\right), & L_1^u > L_c^u \end{cases} \tag{4}$$

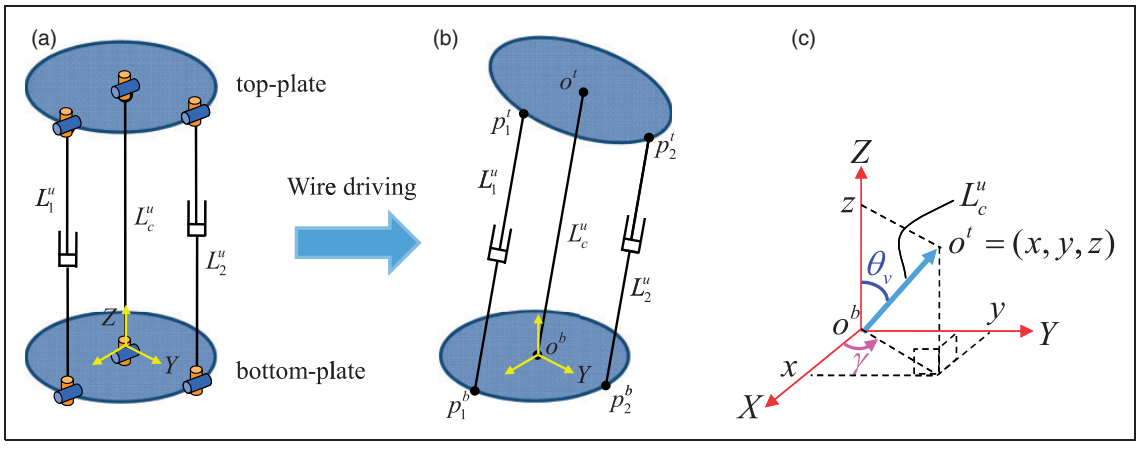

Figure 5. Spatial model of the unit spring backbone. (a) Initial shape of the unit spring backbone. (b) The bent shape of the unit spring backbone. (c) Orientation of the center line L_c^u of the unit spring backbone with respect to XYZ coordinate system.

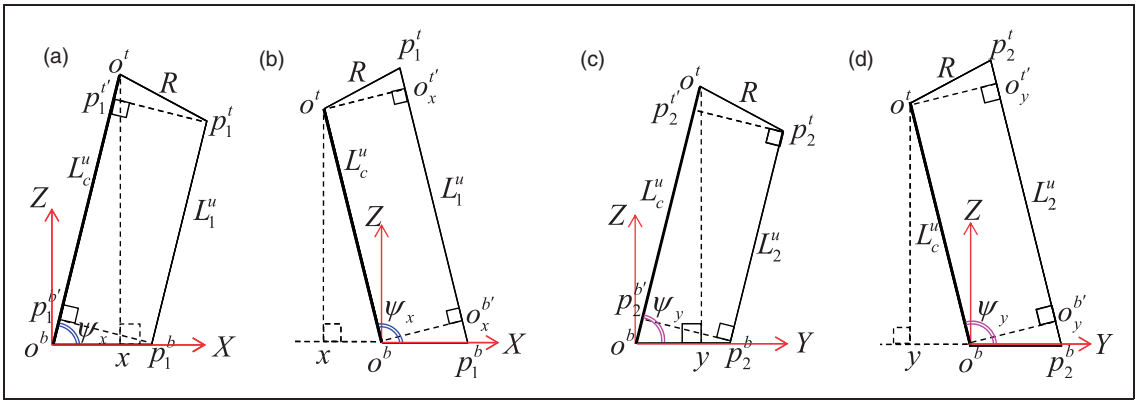

Figure 6. Two isosceles trapezoid ($o^t p_1^t p_1^b o^b$ and $o^t p_2^t p_2^b o^b$) when the unit spring backbone is bent. (a) $o^t p_1^t p_1^b o^b$ when $L_1^u < L_c^u$. (b) $o^t p_1^t p_1^b o^b$ when $L_1^u > L_c^u$. (c) $o^t p_2^t p_2^b o^b$ when $L_2^u < L_c^u$. (d) $o^t p_2^t p_2^b o^b$ when $L_2^u > L_c^u$.

$$\psi_y = \begin{cases} \cos^{-1}\left(\overline{o^b p_2^{b'}}/R\right), & L_2^u < L_c^u \\ 180^\circ - \cos^{-1}\left(\overline{p_2^b o_y^{b'}}/R\right), & L_2^u > L_c^u \end{cases} \quad (5)$$

It is noted from Figure 5(c) that by using x, y, and L_c^u, the azimuth angle γ of the bending plane and the bending angle θ_v of the unit spring backbone can be expressed as

$$\gamma = \text{atan2}(y, x) \quad (6)$$

$$\theta_v = 90^\circ - \cos^{-1}\left(\sqrt{x^2 + y^2}/L_c^u\right) \quad (7)$$

Lastly, using the relationship between θ_v and β (given by equation (1)), β is obtained.

This result can be simply extended to the forward position of a multi-unit continuum robot because it is just a superposition of the forward solution of each unit module. Thus, it is claimed that the proposed continuum robot, constructed by multiple continuum units, possesses a unique forward kinematic solution, although its kinematic structure is similar to a hybrid structure constructed by multiple parallel mechanisms, which usually has multiple forward kinematic solutions.

Design of a master device to control a 4-DOF continuum robot

Tables 1 and 2 show the specifications of the master device. The device has the same kinematic structure as the slave robot, but its design is slightly different from the slave mechanism in terms of the number of nodes. In order to grasp the master device conveniently, the cylinder size is enlarged, and the number of nodes of the master device is less than that of the slave device (to reduce the weight). However, the kinematic mapping between the master device and the slave device is not affected by using a different number of nodes.

Table 1. Specifications of the master device.

Specification	First module (base)	Second module
Diameter	20 mm	20 mm
Length	100 mm	84.5 mm
Cylinder material	Acetal (POM)	Acetal (POM)
Cylinder Length	31 mm	31 mm, 15 mm
Number of nodes	2	2
Wire	SUS304, 7 × 7, diameter: 0.45 mm	
Encoder	Model: E2-512-157-N-D-D-B, US Digital Co.	
	PPR: 512 (Counts per a turn of the pulley is 2048)	

Table 2. Specifications of the unit spring backbone of master device.

	Specification			
Module	K	Length	Diameter	Thickness
First module (base)	0.3 N/mm	19 mm	16 mm	1.0 mm
Second module	0.3 N/mm	19 mm	16 mm	1.0 mm

Figure 7 shows the design of the 4-DOF master device to control the 4-DOF flexible continuum robot. The device consists of two continuum modules, and each module has two nodes. As shown in Figure 7(b), the cylinder has many holes to pass wires through. Additionally, there are two supporting surfaces inside the cylinder to fix a spring between two neighboring cylinders, as shown in Figure 7(c). A pretension of 0.6 N is applied to the wires. We used SUS wire, which is very inextensible as compared to Nylon wire. This is done to avoid stretching (plastic elongation) of the wires. Also, friction between the wires and the cylinders is negligible because the cylinders

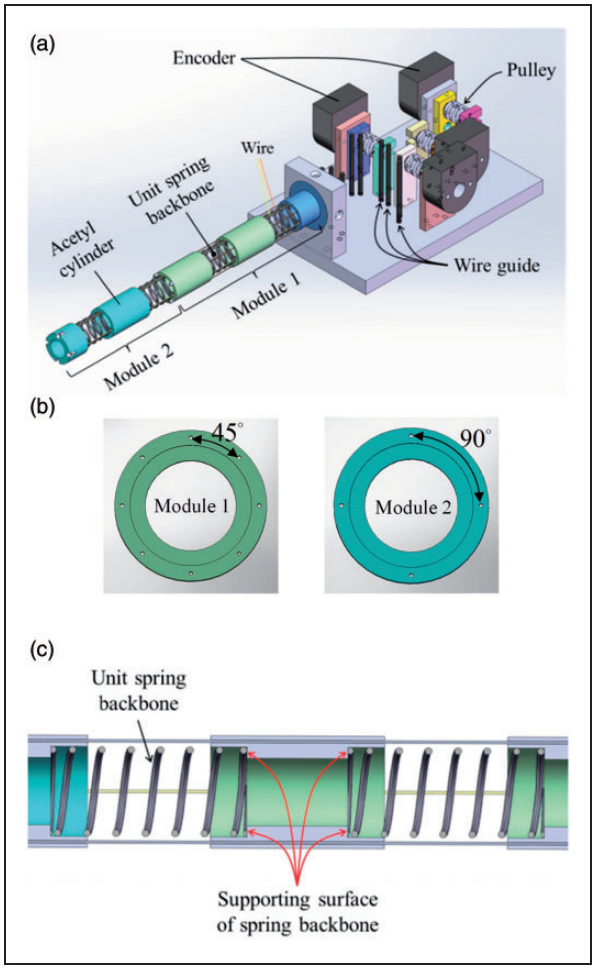

Figure 7. Design of the 4-DOF master device. (a) Assembled state. (b) Cross-sectional view of a cylinder (front). (c) Cross-sectional view of a cylinder (side).

are made of acetal, which is smooth. The initial length of the whole structure is 184.5 mm, and its diameter is 20 mm. Each module is driven by four wires, which pass through holes pierced in the cylinders. The system has four rotary encoders in order to obtain the lengths of the wires in the two modules.

To prevent interference between the eight wires, the heights of the four pulleys are different from each other and wire guides are used. Figure 8 shows the wire arrangement of the 4-DOF master device. Wires that are the same color are coupled.

Implementation

Simulation for the forward kinematic solution

We perform simulation for one continuum module that has two DOF. This is done by using the kinematic model derived in Forward Kinematics of a 4-DOF Continuum Robot section, as shown in Figure 9. Figure 10 shows the simulation results of the forward kinematic solution. It is verified that a unique forward kinematic solution exists for the given input variables.

Hardware setup

To implement an embedded master-slave system, two embedded systems are developed. One consists of a main controller, two 2-axis motion controllers, and four actuators with encoders. The other system consists of a main controller and two sub-controllers, which have two encoder counters, respectively. Figure 11 shows the entire picture of the master and slave system.

A block diagram for the system is shown in Figure 12. The master system and the slave system are connected to each other through the CAN protocol. The operation of the entire system is as follows.

1. At first, when a user controls the master device, the main controller of the master system obtains sensor information from the encoders.
2. Using the sensor information (encoder), the controller calculates the wire length and finds the forward kinematic solution of the master device.
3. Then, the main controller transmits the forward kinematic solution to the slave system. The data transmission rate from the master device to the slave robot is measured to be 1 ms, but it takes only 140 μs to calculate the forward kinematic solution, as shown in Figure 13.
4. When the slave system receives the data, the main controller calculates the inverse kinematic solution and transmits the calculated output of the slave robot to the motion board.

Experimental results

Slave robot control using the master device. Using the 4-DOF master-slave system, we first performed an experiment in which the slave continuum robot is controlled by using the master device. Figure 14 shows that the slave robot successfully follows the movement of the master device. There are several options available to the user. The user can grip the end point (Figure 14(a)) or any arbitrary position (Figure 14(b) through Figure 14(e)) of the robot body to generate a desired configuration of the continuum body. In prior works, a joystick or a commercial haptic device (such as Phantom Omni) has typically been used as the master device. However, since the goal of the proposed master device is to control the whole shape of the continuum robot, a joystick or a commercial haptic device does not easily provide that ability. Since the kinematic structures of those master devices are different from that of the slave robot, the motion-matching between the master and the slave is complex. Thus, easy matching between the master and the slave is preferable. The master device proposed in this work has the same kinematic structure as the slave robot. In other words, the slave robot replicates the motion of the master device. The attached video clip demonstrates such experimental results.

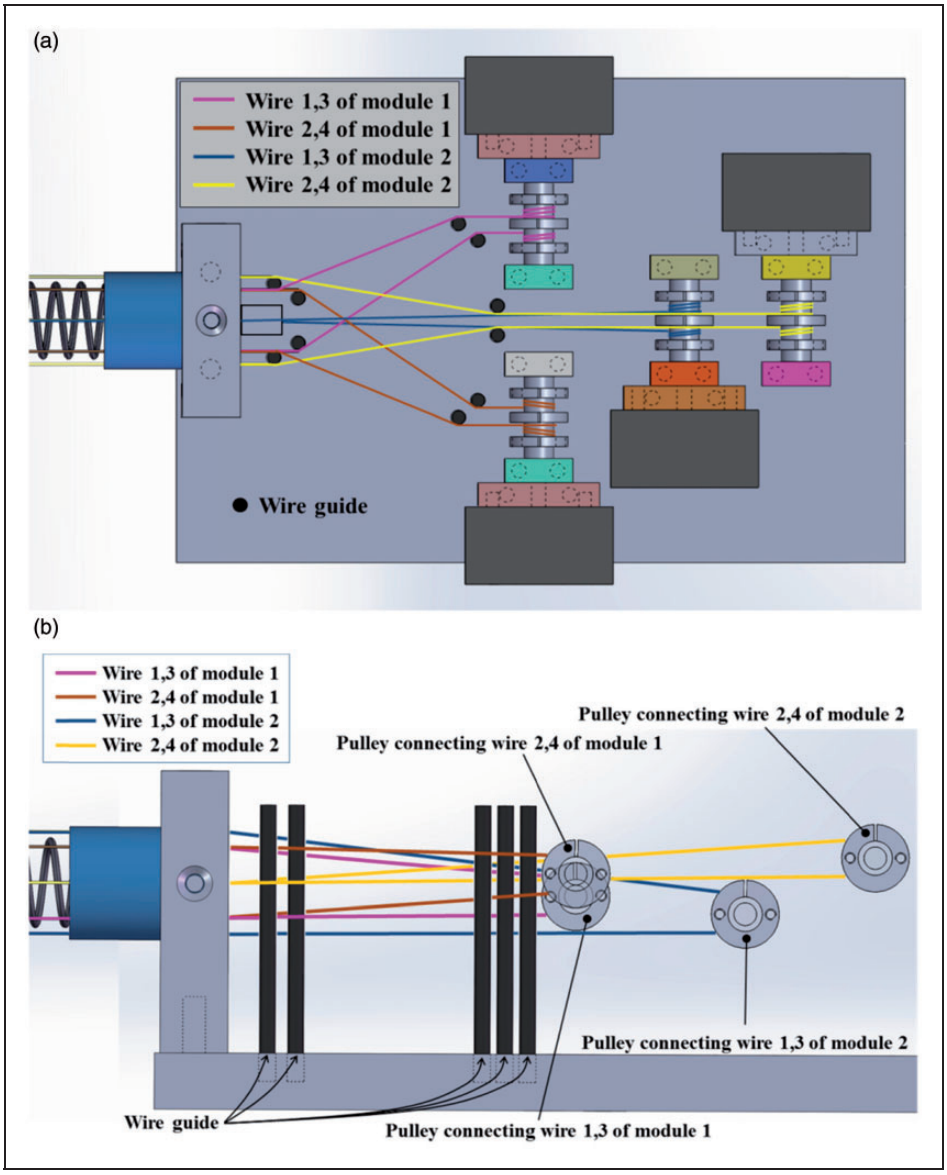

Figure 8. Wire arrangement of the 4-DOF master device. (a) Top view. (b) Side view.

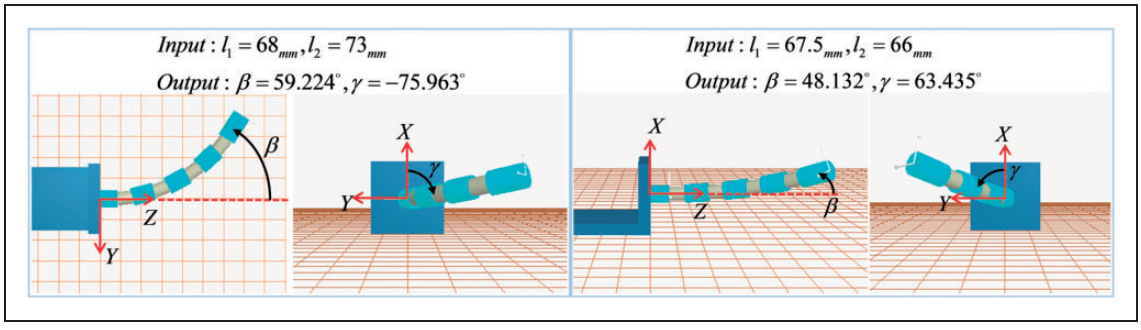

Figure 9. Simulation for the forward kinematic solution.

Inspection of a narrow space using the master-slave system with a micro CCD camera. Additionally, in order to prove that the proposed master device is appropriate for controlling a continuum slave robot, we perform an experiment in which the slave robot avoids obstacles and inspects a narrow area. This is done by using the master-slave continuum robot system equipped with a micro Charge-Coupled Devise (CCD) camera. Three users participated in this experiment. The process used for the inspection is shown in Figure 15.

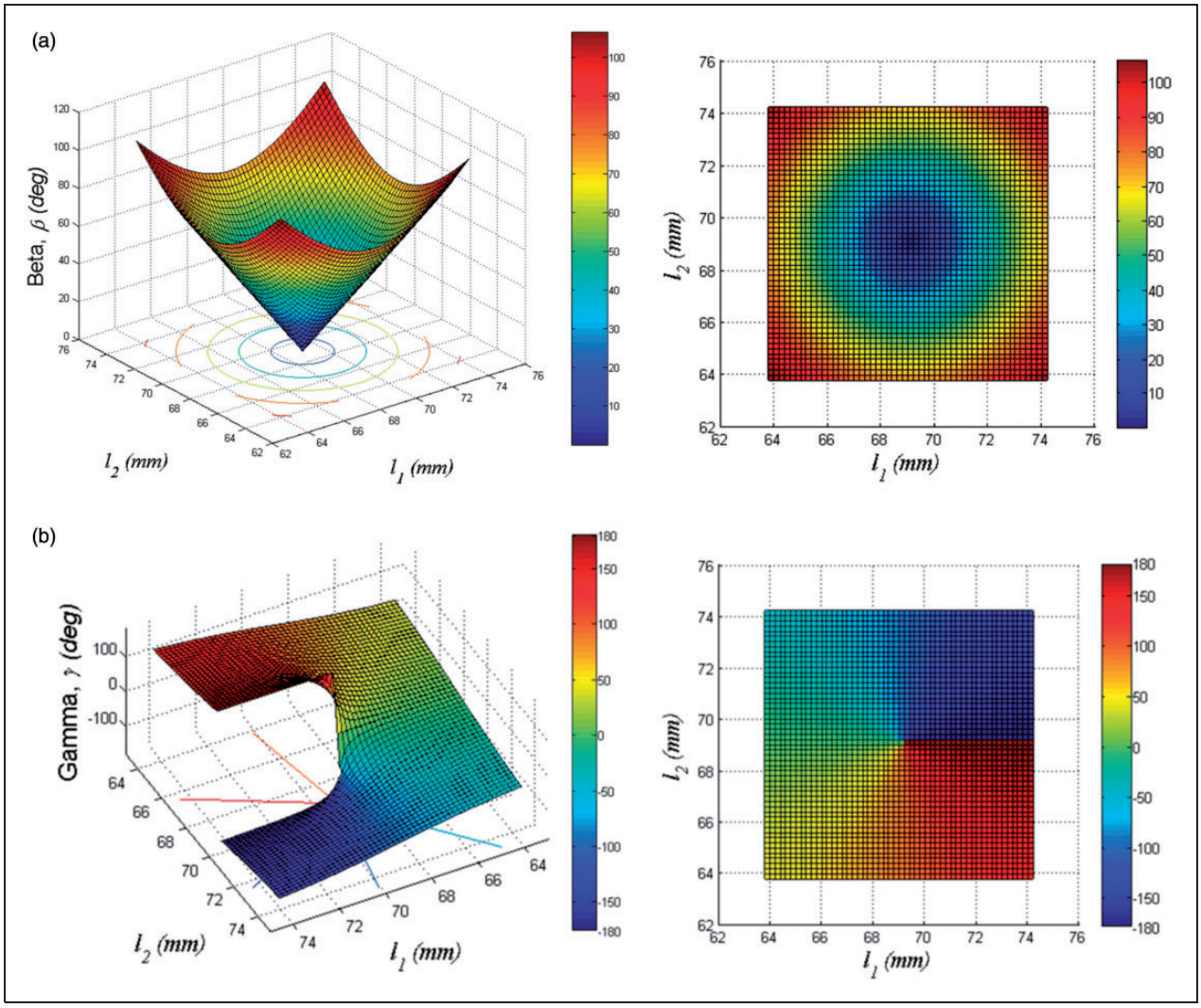

Figure 10. The plot for the forward kinematic solution of a continuum module. (a) Bending angle, β. (b) Rotation angle, γ.

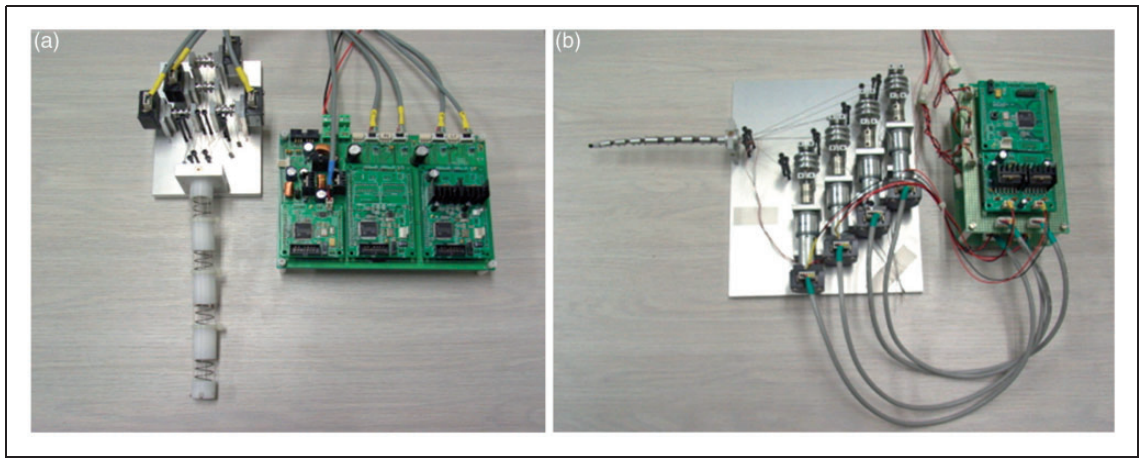

Figure 11. 4-DOF Master-slave system. (a) Master device. (b) Slave robot system.

First, when a user grips and bends the distal continuum module of the master device, the distal module of the slave robot is bent. In that state, the user bends the proximal continuum module of the master device so that the distal end of the slave robot reaches the entrance of a cave. Next, by precisely bending the distal continuum module of the master device, the user inserts the distal end of the slave robot in a way that allows the micro CCD camera to read the text on the wall of the cave. Finally, a user controls

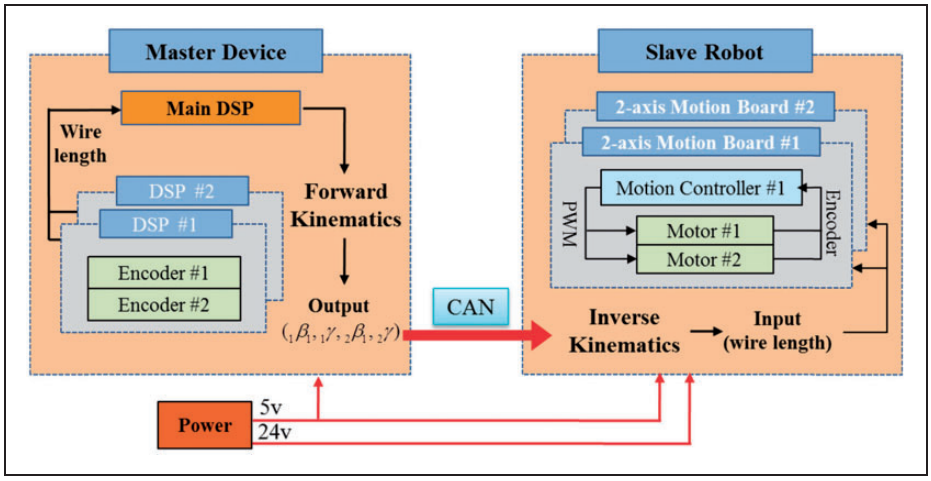

Figure 12. System block diagram.

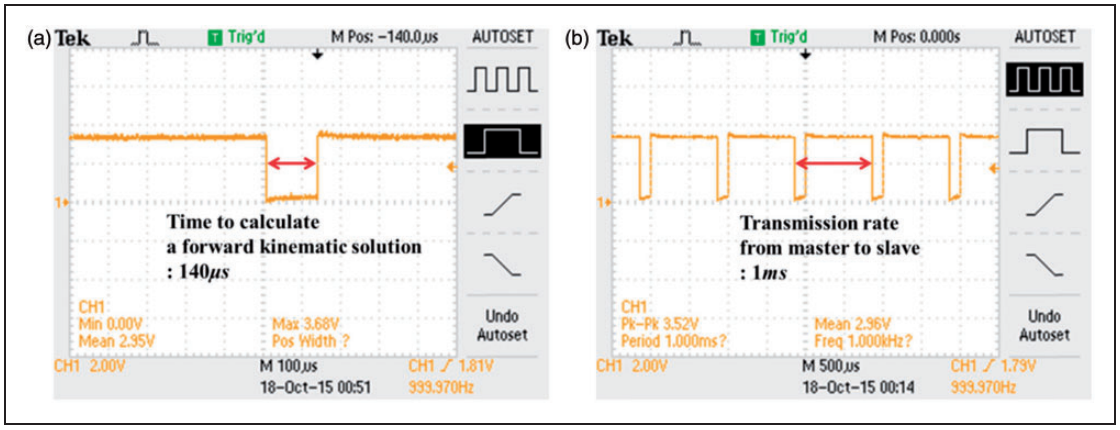

Figure 13. The computation time for a forward kinematic solution. (a) Time to calculate the forward kinematic solution. (b) Transmission rate from master to slave.

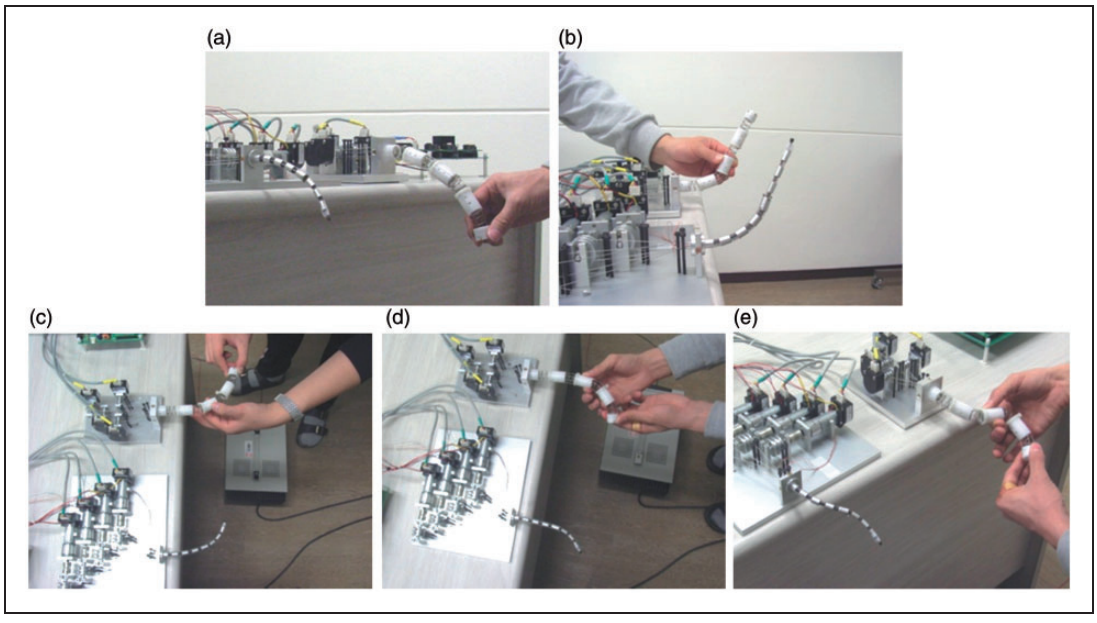

Figure 14. Experimental results of the continuum robot by using the master-slave system. (a) End point control. (b) Arbitrary point control. (c)–(e) Configuration control.

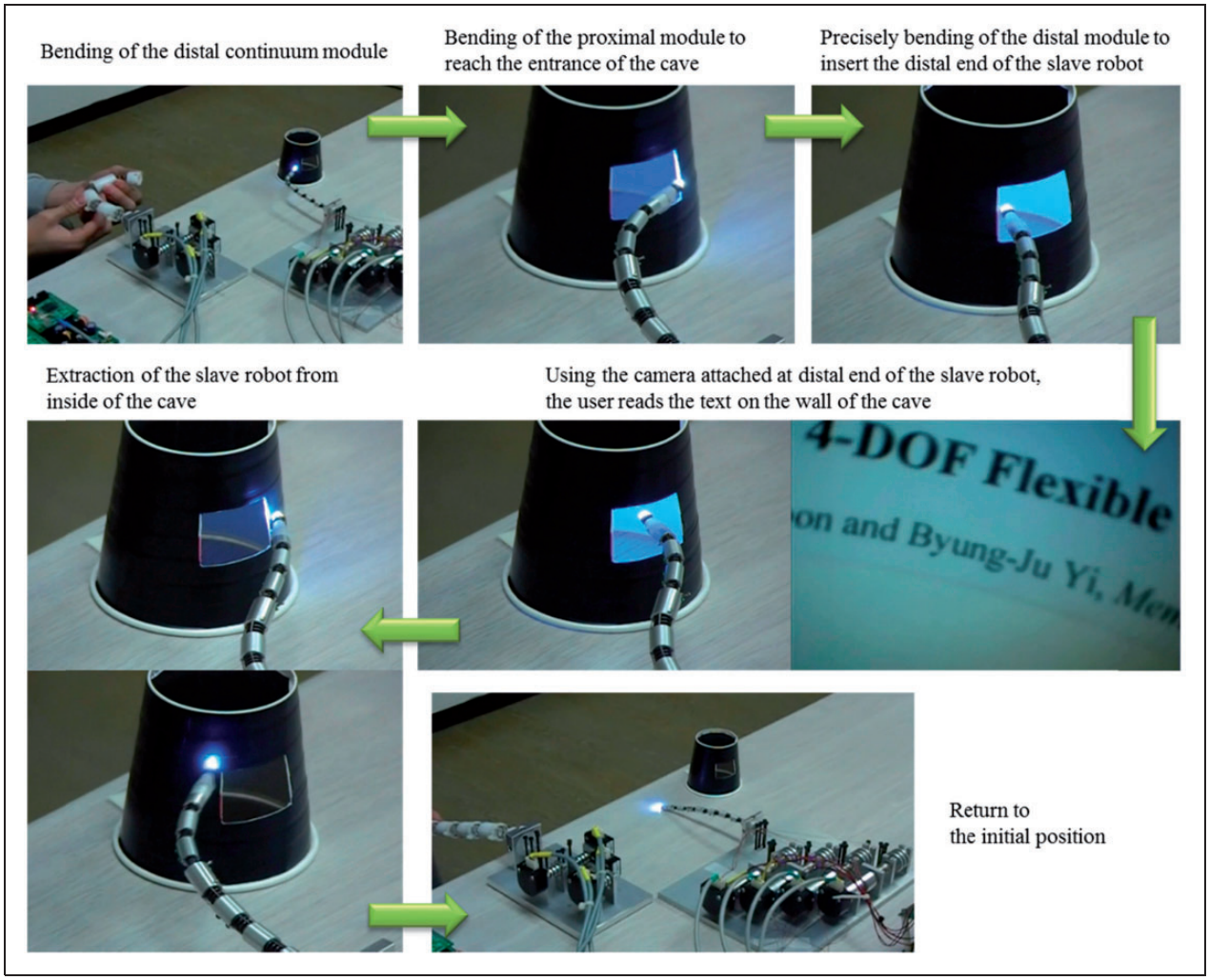

Figure 15. Inspection of a narrow space by using the master-slave system.

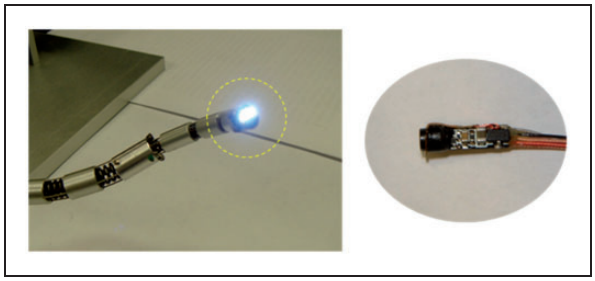

Figure 16. 4-DOF continuum robot with a micro CCD camera.

Table 3. Specifications of micro CCD camera.

Effective pixels	76,800
Resolution	320 × 240
Video outputs	Composite (PAL/NTSC)
Dimension	<Camera head>
	Diameter: 3 mm
Power input	DC 5 V
Field of view	60°

the master device to extract the slave robot from inside of the cave and returns the master device to the initial position. All three users succeeded in the given task; the average completion time for the given task was less than 25 s. The users reported that they felt comfortable using the master device because the kinematic structure of the slave continuum robot is the same as that of the master device.

Compared to typical haptic devices that control the motion of rigid-link robot devices, the proposed master device can control the vibratory motion of the slave device as well as various dexterous motions of the continuum mechanism; these capabilities are enabled by the flexible structure of the spring backbone mechanism. The attached video clip demonstrates such experimental results.

Figure 16 shows the micro CCD camera that was used in this experiment. It is 3 mm in diameter and has a light source installed around the camera lens. The specifications of the CCD camera are included in Table 3.

Conclusion

In this work, we presented a master device for controlling multi-unit continuum robots. The design was introduced and the unique forward kinematic solution for this mechanism was provided. The proposed master device was successfully implemented to control a 4-DOF continuum robot. In the future, we plan to implement a force reflection method to this system.

Declaration of Conflicting Interests

The author(s) declared no potential conflicts of interest with respect to the research, authorship, and/or publication of this article.

Funding

The author(s) disclosed receipt of the following financial support for the research, authorship, and/or publication of this article: This work was supported by the Technology Innovation Program (10040097) funded by the Ministry of Trade, Industry and Energy Republic of Korea (MOTIE, Korea), supported by Mid-career Researcher Program through NRF grant funded by the MEST (NRF-2013R1A2A2A01068814), and supported by the Technology Innovation Program (10049789, Steering and driving mechanism for Cardio-vascular intervention procedure) funded by the Ministry of Trade, Industry & Energy (MOTIE, Korea). This work performed by ICT-based Medical Robotic Systems Team of Hanyang University, Department of Electronic Systems Engineering was supported by the BK21 Plus Program funded by National Research Foundation of Korea (NRF).

References

1. Ikuta K, Hasegawa T and Daifu S. Hyper redundant miniature manipulator "Hyper Finger" for remote minimally invasive surgery in deep area. *Proc IEEE Int Conf Robot Autom* 2003; 1098–1102.
2. Ikuta K, Yamamoto K and Sasaki K. Development of remote micro surgery robot and new surgical procedure for deep and narrow space. *Proc IEEE Int Conf Robot Autom* 2003; 1103–1108.
3. Xu K and Simaan N. Actuation compensation for flexible surgical snake-like robots with redundant remote actuation. *Proc IEEE Int Conf Robot Autom* 2006; 4148–4154.
4. Xu K and Simaan N. An investigation of the intrinisic force sensing capabilities of continuum robots. *IEEE Trans Robot* 2008; 24: 576–587.
5. Goldman RE, Bajo A, MacLachlan LS, et al. Design and performance evaluation of a minimally invasive telerobotic platform for transurethral surveillance and intervention. *IEEE Trans Biomed Eng* 2013; 60: 918–925.
6. Camarillo DB, Milne CF, Carlson CR, et al. Mechanics modeling of tendon-driven continuum manipulators. *IEEE Trans Robot* 2008; 24: 1262–1273.
7. Hannan MW and Walker ID. Kinematics and the implementation of an elephant's trunk manipulator and other continuum style robots. *J Robot Syst* 2003; 20: 45–63.
8. Gravagne IA and Walker ID. Manipulability, force, and compliance analysis for planar continuum manipulators. *IEEE Trans Robot Autom* 2002; 18: 263–273.
9. Jones BA and Walker ID. Kinematics for multisection continuum robots. *IEEE Trans Robot* 2006; 22: 43–55.
10. Hannan MW and Walker ID. Analysis and initial experiments for a novel elephant's trunk robot. *Proc IEEE/RSJ Int Conf Intell Robot Syst* 2000; 330–337.
11. Hannan MW and Walker ID. Novel kinematics for continuum robots. *Proc Adv Robot Kinematics* 2000; 227–238.
12. Webster RJ III, Romano JM and Cowan NJ. Mechanics of precurved-tube continuum robots. *IEEE Trans Robot* 2009; 25: 67–78.
13. Gilbert HB, Neimat J and Webster RJ III. Concentric tube robots as steerable needles: achieving follow-the-leader deployment. *IEEE Trans Robot* 2015; 31: 246–258.
14. Webster RJ, Romano JM and Cowan NJ. Mechanics of precurved-tube continuum robots. *IEEE Trans Robot* 2009; 25: 67–78.
15. Rucker DC and Webster RJ III. A telerobotic system for transnasal surgery. *IEEE/ASME Trans Mechatron* 2014; 19: 996–1006.
16. Mahvash M and Dupont PE. Stiffness control of surgical continuum manipulators. *IEEE Trans Robot* 2011; 27: 334–345.
17. Choi D-G, Yi B-J and Kim WK. Design of a spring backbone micro endoscope. *Proc IEEE/RSJ Int Conf Intell Robot Syst* 2007; 1815–1821.
18. Yoon H-S, Oh SM, Jeong JH, et al. Active bending endoscope robot system for navigation through sinus area. *Proc IEEE/RSJ Int Conf Intell Robot Syst* 2011; 967–972.
19. Yoon H-S, Cha H-J, Chung J, et al. Compact design of a dual master-slave system for maxillary sinus surgery. *Proc IEEE/RSJ Int Conf Intell Robot Syst* 2013; 5027–5032.
20. Csencsits M, Jones BA, McMahan W, et al. User interfaces for continuum robot arms. *Proc IEEE/RSJ Int Conf Intell Robot Syst* 2005; 3011–3018.
21. Yoon H-S and Yi B-J. A 4-DOF flexible continuum robot using a spring backbone. *Proc Int Conf Mechatron Autom* 2009; 1249–1254.
22. Yoon H-S, Jeon J, Chung J, et al. A continuum module for developing a biopsy device. *Proc Int Conf Ubiquitous Robot Ambient Intell* 2012; 442–444.

Appendix 1

Notation

L_c	center line of continuum unit module
L_s	length of inner boundary in the planar continuum model
L_l	length of outer boundary in the planar continuum model
l_i	length of ith wire
L_c^u	center distance between two neighboring cylinders
L_s^u, L_l^u	unit lengths of L_s and L_l
L_i^u	length of ith wire in the spatial model of the unit spring backbone
${}_m\beta_1$	bending angle of mth continuum unit module

${}_m\gamma$	rotation angle of mth continuum unit module
${}_m l_i$	length of ith wire of mth continuum unit module
N	the number of nodes in one continuum unit module
O_p	center of curvature of unit spring backbone
o^t	center of the top-plate in spatial model of the unit spring backbone
o^b	center of the bottom-plate in spatial model of the unit spring backbone
p_i^t	location of ith wire passed through the top-plate in the spatial model of the unit spring backbone
p_i^b	location of ith wire passed through the bottom-plate in the spatial model of the unit spring backbone
R	distance between the center of the cylinder and the wire hole in the cross-sectional view of the cylinder
β_1	bending angle of continuum unit module
γ	rotation angle of continuum unit module (azimuth angle of the bending plane)
ψ_x	angle between x-axis on the bottom-plate and $\overline{o^b o^t}$
ψ_y	angle between y-axis on the bottom-plate and $\overline{o^b o^t}$